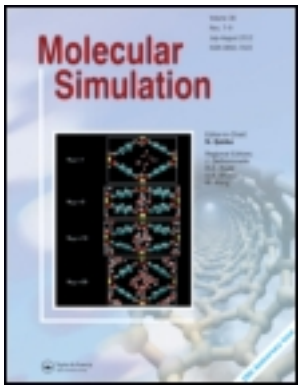

Molecular Simulation
Publication details, including instructions for authors and subscription information:
http://www.tandfonline.com/loi/gmos20

Classical and 3D QSAR studies on inverse agonists of human histamine H1 receptor

Sundarapandian Thangapandian [a], Shalini John [a] & Keun Woo Lee [a]

[a] Division of Applied Life Science (BK21 Program), Systems and Synthetic Agrobiotech Center (SSAC), Plant Molecular Biology and Biotechnology Research Center (PMBBRC), Research Institute of Natural Science (RINS), Gyeongsang National University (GNU), 501 Jinju-daero, Gazha-dong, Jinju, 660-701, Republic of Korea

Version of record first published: 20 Sep 2012.

To cite this article: Sundarapandian Thangapandian, Shalini John & Keun Woo Lee (2012): Classical and 3D QSAR studies on inverse agonists of human histamine H1 receptor, Molecular Simulation, 38:13, 1143-1156

To link to this article: http://dx.doi.org/10.1080/08927022.2012.696638

Molecular Simulation
Vol. 38, No. 13, November 2012, 1143–1156

Classical and 3D QSAR studies on inverse agonists of human histamine H1 receptor

Sundarapandian Thangapandian, Shalini John and Keun Woo Lee*

Division of Applied Life Science (BK21 Program), Systems and Synthetic Agrobiotech Center (SSAC), Plant Molecular Biology and Biotechnology Research Center (PMBBRC), Research Institute of Natural Science (RINS), Gyeongsang National University (GNU), 501 Jinju-daero, Gazha-dong, Jinju 660-701, Republic of Korea

(*Received 29 November 2011; final version received 20 May 2012*)

Human histamine H1 receptor (HHR1) is one of the receptors through which histamine exerts its allergic reactions, and inhibition of this receptor is an important strategy in treatment of inflammatory diseases. In this study, classical and 3D quantitative structure–activity relationship (QSAR) studies were carried out using 36 inverse agonists of which 27 diverse compounds were used in training set. The MOE® and SYSTAT® programs were used in descriptor calculation and step-wise multiple regression analysis. A predictive and statistically significant QSAR model based on four descriptors was developed and cross-validated with the leave-one-out (LOO) method. The statistical data of this model were $r = 0.908$, $F = 25.703$, $s = 0.445$, $q^2_{LOO} = 0.945$. Comparative molecular field analysis (CoMFA) and comparative molecular similarity indices analysis (CoMSIA) studies were carried out using the same training set compounds. Pharmacophore-based molecular alignment was used to develop models using different fields. The best CoMFA model was the one developed using the CoMFA indicator fields ($r^2 = 0.998$, $q^2_{LOO} = 0.580$), and the best CoMSIA model was the one with CoMSIA steric fields ($r^2 = 0.862$, $q^2_{LOO} = 0.434$). As the models explain well the observed variance in HHR1 binding affinities in both the training and the test set, they can be used in designing future antihistamines.

Keywords: CoMFA; CoMSIA; contour maps; human histamine H1 receptor; inverse agonists

1. Introduction

Quantitative structure–activity relationship (QSAR) is a method building computational or mathematical models that can derive a statistically significant correlation or relationship between physicochemical properties and biological activities of chemical substances and used in the prediction of new chemical entities. The physicochemical properties refer here to the structure of the chemical compounds, and the statistical methods such as regression analysis, partial least square (PLS) analysis, principal components analysis, neural networks and genetic algorithms are used in deriving significant models. The basic principle behind QSAR is that the difference in structural properties is responsible for the observed changes in biological activities of the compounds [1]. Various QSAR approaches were developed in the course of time and have been considered as valuable tools in designing new pharmaceuticals and agrochemicals. Early and classical QSAR studies have utilised 1D and 2D structural properties, and this was considered as a major drawback of this type for which 3D QSAR method was considered as replacement in which 3D properties of the ligands are used to predict the biological activities. Despite these types, all QSAR methods focus on the same goals which are as follows: (i) quantification of the structural properties that directly influence the biological activities, (ii) optimisation of existing leads to improve their biological activities and (iii) prediction of biological activities of untested and newly designed compounds. The QSAR techniques have always been considered as good alternatives to the drug discovery and development scientists as it can reduce the cost and time of conventional syntheses and biological assays. The 1D and 2D QSAR methods correlate biological activities with global molecular properties such as pK_a and log P and structural patterns such as connectivity indices and 2D pharmacophores. But the 3D QSAR method is a broad category including all those QSAR methods that correlate the biological activity with non-covalent interaction fields surrounding the compounds and computed atom-based descriptors calculated from the spatial representation of the molecular structures [2–5].

Histamine receptors are categorised under the superfamily of G-protein-coupled receptors (GPCRs). GPCRs transduce signals across the cell membrane upon ligand binding (a photon in case of opsins), and at the cytosolic side they activate the G-protein. GPCR consists of a single protein that crosses the cell membrane seven times. Human histamine H1 receptor (HHR1) belongs to class I of the GPCRs and interacts with G-proteins to activate phospholipase C [6]. Ligands bind on the extra cellular part of the membrane and transduce the signal. Four subtypes (H1–H4) of histamine receptors are present in various parts of human body which deliver various actions

*Corresponding author. Email: kwlee@gnu.ac.kr

ISSN 0892-7022 print/ISSN 1029-0435 online

http://dx.doi.org/10.1080/08927022.2012.696638
http://www.tandfonline.com

against ligand binding [7–16]. Specific activation or blockade of these receptor subtypes has led to a tremendous increase in the knowledge of the roles of histamine in both physiology and pathology. HHR1 is known to be involved in various inflammatory effects [17]. Moreover, histamine plays a role in allergic conditions that have often been treated successfully with HHR1 antagonists [18]. It is reported majorly that GPCRs are activated even in the absence of agonists and this phenomenon is known as constitutive receptor activity and compounds blocking this activity are called inverse agonists [19]. Early research and development of HHR1 ligands started on antagonists that were used for their anti-allergic effects in the periphery. However, the first generation HHR1 antagonists such as mepyramine (MEP) and diphenhydramine have exhibited Central Nervous System (CNS)-related side effects due to their high lipophilicity [20–22]. This was followed by the development of second generation HHR1 antagonists such as acrivastine and cetirizine, which exhibited high selectivity and less sedative effect due to the decrease in their ability to penetrate blood–brain barrier [23,24]. A non-selective nature of some of this class of compounds was observed as they have also shown affinity towards 5-HT_{2A}, dopamine D2 and muscarinic M1 receptors [25]. Zwitterionic HHR1 antagonists such as acrivastine and fexafenadine have shown the highest degree of selectivity for HHR1. The inverse agonism has become a well-accepted phenomenon in the field of GPCRs [26–30]. Many ligands that were previously thought to act as antagonists actually inhibit constitutive receptor signalling, indicating their inverse agonistic behaviour. It was reported that there are various human diseases as the results to constitutive receptor activity induced by mutations in genes encoding GPCRs [31–34]. From this it has become obvious that for these genetic disorders, inverse agonists are necessary to treat the mutant GPCRs, as other antagonists would be of no use. Thus, the development of HHR1 inverse agonists will become an effective pharmacological means to study the constitutive activity of HHR1 and to address the problems arisen due to this activity. As very limited SAR studies have been reported in these molecules, in this study, systematic classical and 3D QSAR studies were carried out in order to identify the essential structural features and physicochemical properties that correlate the inverse agonistic properties of the ligand molecules.

In our QSAR studies, a set of diverse compounds with alkylaminoimidazoles, alkylaminopyridines, thiazoles and various other alkylamines were utilised to generate classical and 3D QSAR models. Comparative molecular field analysis (CoMFA) models were developed using different fields, viz. Tripos Standard, hydrogen bonding and parabolic indicator, whereas comparative molecular similarity indices analysis (CoMSIA) models were developed using steric, electrostatic, donor, acceptor, hydrophobic and combination of fields. The generated models were further validated using an external test set by predicting the biological activities of the test set compounds. The contour maps derived from CoMFA and CoMSIA models were the visual results of SAR observed from the data-set of compounds with biological activities. The SAR information extracted from these models could effectively be used in HHR1 inverse agonist designing.

2. Materials and methods

2.1 Selection of data-sets

A set of 36 diverse chemical compounds with a wide range of experimentally known inverse agonistic activities for HHR1 were used in this study. Classical and 3D QSAR approaches were employed to observe the SAR within the selected set of HHR1 inverse agonists. The activity values of the compounds ranged from 0.002 to 501.18 μM over five orders of magnitude (Table 1). The compounds under study include derivatives of aminoalkylimidazoles, aminoalkylthiazoles, aminoalkylpyridines and arylalkylamines. The binding affinity data of these compounds for HHR1 are expressed in K_i values, which were determined under the same biological conditions [35]. The selection of training set is considered very important for any QSAR technique as that influence the model generation directly and as equal is the test set utilised in model validation. Thus, this data-set was divided into training and test sets based on their chemical diversity and activity. The resultant training and test sets represented the full range of activity values. Particularly, the molecules with lowest and highest activity were selected to be in the training set. Whereas the training set used in model generation test set was used in validating or testing the predictive ability of the generated models.

2.2 Classical QSAR

Molecular operating environment (MOE) Version 2005.06 software from Chemical Computing Group was used for sketching, minimising the energy of the molecules and calculating various physicochemical descriptors [36]. MOE is a fully integrated suite of computational chemistry, molecular modelling and informatics software for various life science applications. MOE runs on a wide range of computer hardware, including computer clusters, making it ideal for use by experts and occasional users alike. Two-hundred and thirty-five molecular descriptors available in MOE were calculated using its *QSAR descriptors* module. The resultant file was saved in MS-excel format to be comfortably used with other computational and statistical programs. Other programs, namely SYSTAT 10.2 [37] and BuildQSAR [38], were employed to perform various statistical calculations with the data. The correlation matrix

Table 1. Training and test set compounds.

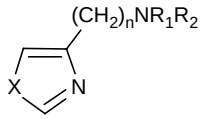

Name	X	*n*	R_1	R_2	pK_i	K_i (μM)
1a	NH	6	H	H	3.3	501.19
1b	NH	8	H	H	4.4	39.81
1c	NH	9	H	H	4.7	19.95
1d	NH	10	H	H	5.3	5.01
1e[a]	NH	11	H	H	5.6	2.51
1f	NH	12	H	H	6	1.00
1 g	NH	13	H	H	6.4	0.40
1 h	NH	14	H	H	6.6	0.25
1i	NH	8	$-(CH_2)_4-$		5.4	3.98
1j[a]	NH	10	$-(CH_2)_4-$		5.4	3.98
1k	NH	12	$-(CH_2)_4-$		5.7	1.99

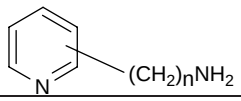

Name	Isomer	*n*	pK_i	K_i (μM)
PEA[a]	*Ortho*	2	3.8	158.49
13a	*Ortho*	9	4.5	31.62
13b[a]	*Ortho*	10	4.9	12.59
13c	*Ortho*	12	6	1.00
13d	*Meta*	10	5.1	7.94
13e[a]	*Meta*	12	5.4	3.98
13f	*Para*	10	5.3	5.01
13 g	*Para*	12	5.4	3.98

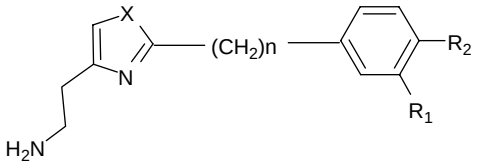

Name	*X*	*N*	R_1	R_2	pK_i	K_i (μM)
17a	NH	0	Cl	H	5.2	6.31
17b	NH	0	CF_3	H	5.4	3.98
17c	NH	0	Cl	Cl	4.7	19.95
19a[a]	S	0	H	H	4.5	31.62
19b	S	0	CF_3	H	4.9	12.59
19c	S	1	H	H	4.2	63.10
19d	S	1	Cl	H	4.5	31.62

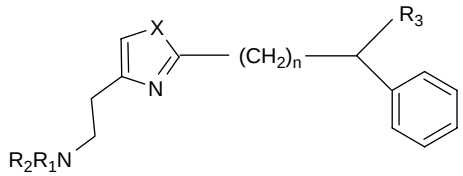

Name	*N*	R_1	R_2	R_3	pK_i	K_i (μM)
18b[a]	1	H	H	Phenyl	5.1	7.94
18c	2	H	H	Phenyl	5.7	1.99
18d	3	H	H	Phenyl	5.8	1.59
18e[a]	4	H	H	Phenyl	5.9	1.26
18f	2	H	H	Cyclohexyl	5	10.00
18 g	2	H	H	*p*-Br-phenyl	5.6	2.51
18 h	2	H	H	*p*-CH_3-phenyl	5.5	3.16
18i	2	$-(CH_2)_4-$		Phenyl	5.6	2.51

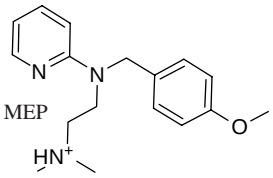

$pK_i = 8.7$ ($K_i = 0.002\ \mu M$)

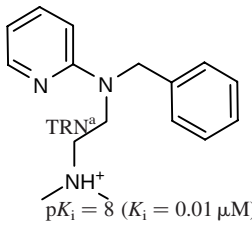

$pK_i = 8$ ($K_i = 0.01\ \mu M$)

[a] Test set compounds.

generation and multiple linear regression (MLR) analyses were carried out using SYSTAT and the q^2, which is also known as cross-validated correlation coefficient; calculation was carried out in BuildQSAR program. The MLR is also known as linear free-energy relationship method, which is an extension of simple linear regression analysis to more than one dimension [39]. MLR generates QSAR equations by performing standard multivariable regression calculations to identify the dependence of a drug property on any or all of the descriptors under investigation. The possibility of chance correlation is checked through the values of multiple correlation coefficients (r), Fisher's F ratio, standard deviation (s) and through independent tests such as the leave-one-out (LOO) method. The significance of correlation can be judged through q^2 values. Step-wise MLR method is a commonly used variant of MLR which also creates a multiple-term linear equation, but not all the independent variables are used [40]. In contrast to MLR, each independent variable is sequentially added to the equation and new regression is performed every time. The new term is preserved only if the model passes a test for significance. This regression technique is especially useful when the number of descriptors is large and the key descriptors are unknown.

2.3 3D QSAR

CoMFA and CoMSIA were carried out on a Silicon Graphics Octane R12000 workstation running on SYBYL 6.9 molecular modelling software (Tripos, St Louis, MO, USA). The chemical structures drawn using MOE and used in classical QSAR calculations were imported into SYBYL for 3D QSAR calculations. Partial charges were computed using Gasteiger–Huckel method, and were optimised for their geometry using Tripos force field with a distance-dependent dielectric function and energy convergence criterion of 0.001 kcal/mol Å using 1000 iterations and standard SYBYL settings [41,42]. Alignment of the compounds is a crucial step in CoMFA studies, and SYBYL provides three different methods such as maximum common structure-based alignment, rigid body field fit alignment and multifit alignment to generate an alignment of compounds. There are other methods utilising pharmacophore model, and molecular docking was also reported to generate a valid alignment of compounds [1,42–46]. A pharmacophore-based alignment of compounds was generated in this study utilising our HypoGen-based pharmacophore model, which was made of five pharmacophoric features and high predictive ability [19,47].

2.4 CoMFA and CoMSIA model development

CoMFA generates an equation correlating the biological activity with the contribution of interaction energy fields at every grid point. CoMFA results are shown as coefficient contour plots to allow simple and easy visual interpretation. These contour maps explain important regions in space around the molecules where specific modifications significantly alter the activity [47,48]. The alignment of compounds obtained based on the pharmacophore model was further used in CoMFA and CoMSIA studies. In this 3D QSAR method, superimposed molecules are kept in a 3D grid for various calculations. The steric (Lennard-Jonnes potentials) and electrostatic fields (Coulombic potentials) for CoMFA were calculated using fields, viz. standard CoMFA field, H-bonding fields, indicator fields and parabolic fields for the CoMFA calculation. For each alignment, an sp^3 carbon atom having a charge of $+1$ and a radius of 1.52 Å was used as a probe to calculate various steric and electrostatic fields, the grid spacing was set at 2 Å and the region was calculated automatically. In order to investigate the influence of different parameters on CoMFA, various steric and electrostatic cut-offs and grid spacing were also tried.

In the CoMSIA calculation, molecular similarity indices were calculated at different points in a regularly spaced grid for pre-aligned compounds. Several advantages such as greater robustness related to both region shifts and small shifts within the alignments, no application of steric cut-offs and more intuitively interpretable contour maps render CoMSIA much more superior than CoMFA. The standard settings are the probe with charge to $+1$, hydrogen bond accepting to $+1$, attenuation factor α to 0.3 and grid spacing to 2 Å for CoMSIA calculations. This calculates five different fields such as steric, electrostatic, hydrophobic, acceptor and donor.

2.5 PLS analysis

It is an iterative regression procedure that produces its solutions based on linear transformation of a large number of original descriptors to a small number of new orthogonal terms called latent variables [49]. PLS gives a statistically robust solution even when the independent variables are highly interrelated among themselves, or when the independent variables exceed the number of observations. Thus, PLS is able to analyse complex structure–activity data in a more realistic way, and effectively interpret the influence of molecular structure on biological activity. This is one of the standard statistical methods used for the development of predictive 3D QSAR models. All models were investigated using full cross-validated PLS (LOO) method with CoMFA standard options for scaling of variables. Initially, the minimum sigma (column filtering) was set to 2.0 kcal/mol to improve the signal-to-noise ratio by omitting those lattice points the energy variation of which is below this threshold. The statistical significance and predictive ability of the resulting models were assessed using LOO cross-validated r^2, also called q^2. The conventional r^2 was considered as a measure of the predictive ability within the training set, whereas the q^2 was considered as a measure of predictive ability outside the training set.

2.6 Model validation and contour maps

The developed models were validated for their predictive ability over the biological activities of external compounds that were not used in model development. Nine compounds were used as external data-set in the model validation process. Correlation co-efficient values were calculated from the experimental and predicted activity values. The contour maps of CoMFA denote the region in the space where the aligned molecules would favourably or unfavourably interact with the receptor whereas the CoMSIA contribution maps denote those areas within the specified region where the presence of a group with a particular physicochemical property will be favoured or disfavoured for good biological activity. Generally, two types of contours are shown for each interaction energy field: the positive and negative contours. The contours for steric fields are shown in green (positive contours, more bulk favoured) and yellow (negative contours, less bulk favoured), whereas the electrostatic field contours are displayed in red (positive contours, electronegative substituents favoured) and blue (negative contours, electropositive substituents favoured) colours [50].

3. Results and discussion

3.1 Molecular descriptors and classical QSAR model generation

All available molecular descriptors in MOE were calculated and used in QSAR model generation. Pearson correlation matrix displaying inter-correlation between the activity value and all descriptors was calculated using SYSTAT 10.2 (Table 2). Analyses of the inter-correlation values revealed the possible highly correlating descriptors with dependent variable, and thus, they were preferred to be used as independent variables during QSAR model generation using MLR analysis. The biological activity was used as the dependent variable. The descriptors scoring inter-correlation value >0.5 within independent variables were not considered, whereas the descriptors scoring >0.5 with biological activity (dependent variable) were considered in QSAR model generation. None of the descriptors used in deriving final model has shown an inter-descriptor correlation more than 0.205 between independent variables. The following parameters were correlating well with the biological activity rather than any other descriptors without showing any considerable inter-correlations with other descriptors: (i) RINGS representing the number of rings present in the compounds under study, (ii) KierA3 representing third alpha modified shape index, (iii) Q_VSA_PPOS indicating positive polar van der Waals surface area and (iv) E_OOP standing for the out-of-plane potential energy (Tables 3 and 4).

In view of the major contribution to the generated model, the predicted activity values of the compounds are from Q_VSA_PPOS, which represent the positive polar van der Waals surface area. It is of interest to focus our attention to study the contribution of this parameter by every substituent rather than the whole molecule. HHR1 inverse agonist activity (pK_i) also referred to as biological activity was selected as dependent variable in step-wise multi parameter regression analysis, whereas all other structural physicochemical parameters were chosen to be independent variables. Regression analysis led to the

Table 2. Correlation matrix of physicochemical parameters used in model generation.

	BA	RINGS	Q_VSA_PPOS	E_OOP	KierA3
BA	1	0.119	0.641	−0.429	0.339
RINGS		1	0.205	−0.148	−0.576
Q_VSA_PPOS			1	−0.040	−0245
E_OOP				1	−0.189
KierA3					1

Table 3. Calculated descriptors along with the experimental and predicted biological activities of training set compounds (sorted by its pK_i values).

Comp.	pK_i (Exp.)	RINGS	Q_VSA_PPOS	E_OOP	KierA3	pK_i (Pred.)	Residual
1a	3.300	1	39.049	0.031	3.626	3.31	−0.01
19c	4.200	2	44.171	0.000	3.069	4.89	−0.69
1b	4.400	1	39.049	0.000	5.095	4.89	−0.49
13a	4.500	1	30.430	0.000	6.530	4.92	−0.42
19d	4.500	2	44.171	0.001	3.700	5.02	−0.52
17c	4.700	2	39.049	0.000	2.649	4.56	0.14
1c	4.700	1	39.049	0.000	5.832	5.09	−0.39
19b	4.900	2	48.151	0.000	3.066	5.05	−0.15
18f	5.000	3	39.049	0.000	4.167	5.32	−0.32
13d	5.100	1	30.430	0.000	7.305	5.13	−0.03
17a	5.200	2	39.049	0.000	2.294	4.46	0.74
13f	5.300	1	30.430	0.000	7.305	5.13	0.17
1d	5.300	1	39.049	0.000	6.669	5.32	−0.02
13 g	5.400	1	30.430	0.000	8.977	5.59	−0.19
17b	5.400	2	48.095	0.000	2.664	4.94	0.46
1i	5.400	2	48.196	0.001	5.324	5.64	−0.24
18 h	5.500	3	39.049	0.000	4.654	5.45	0.05
18 g	5.600	3	39.049	0.000	4.425	5.39	0.21
18i	5.600	4	48.196	0.000	4.470	6.13	−0.53
18c	5.700	3	39.049	0.002	3.678	5.11	0.59
1k	5.700	2	48.196	0.000	8.067	6.43	−0.73
18d	5.800	3	39.049	0.001	4.120	5.27	0.53
13c	6.000	1	30.430	0.000	8.977	5.59	0.41
1f	6.000	1	39.049	0.000	8.318	5.77	0.23
1 g	6.400	1	39.049	0.000	9.131	6.00	0.40
1 h	6.600	1	39.049	0.000	10.02	6.24	0.36
MEP	8.700	2	122.243	0.000	4.410	8.54	0.16

Notes: MEP, Mepyramine. Residual = predicted activity – experimental activity.

Table 4. Summary of PLS statistics of various CoMFA models using different fields.

Parameters	COMFA_T	COMFA_H	COMFA_I	CoMFA_P
q^2	0.551	0.325	0.580	0.573
r^2	1.000	0.987	0.998	0.998
SE of estimate	0.009	0.128	0.050	0.045
F	39561.614	301.170	2003.80	2474.812
Component	7	5	7	6
Fraction	0.516(s)	0.649(d)	0.646(s)	0.545(s)
	0.484(e)	0.351(a)	0.354(e)	0.455(e)

Notes: CoMFA_T – Tripos, CoMFA_H — Hydrogen bond, CoMFA_I – Indicator, CoMFA_P – Parabolic fields. s, e, a and d are steric, electrostatic, hydrogen bond acceptor and donor field contributions, respectively.

derivation of the following QSAR equation:

$$\begin{aligned} \mathrm{p}K_i =& 1.501(\pm 0.538) + 0.344(\pm 0.128)\,\mathrm{RINGS} \\ &+ 0.042(\pm 0.005)\,\mathrm{Q\_VSA\_PPOS} - 37.816 \\ &\times (\pm 15.864)\,\mathrm{E\_OOP} + 0.275(\pm 0.050)\,\mathrm{KierA3}, \\ & n = 27,\ r = 0.908,\ r^2 = 0.824,\ q^2 = 0.945, \\ & s = 0.445,\ F = 25.703. \end{aligned}$$

This equation shows a high correlation ($r = 0.908$) on HHR1 inverse agonist activity with Q_VSA_PPOS, RINGS, E_OOP and KierA3 descriptors. These are the four best parameters that can fit well with the biological activity. The combination of other descriptors led to the reduced correlation co-efficient and high inter-descriptor correlation. This QSAR model has predicted the pK_i values of the training set compounds with a correlation value (r) of 0.908, and none of the residual values was >0.8 (Table 3 and Figure 1). This prediction and residual values are strong indications of predictive ability of the generated model (Figure 2(a)).

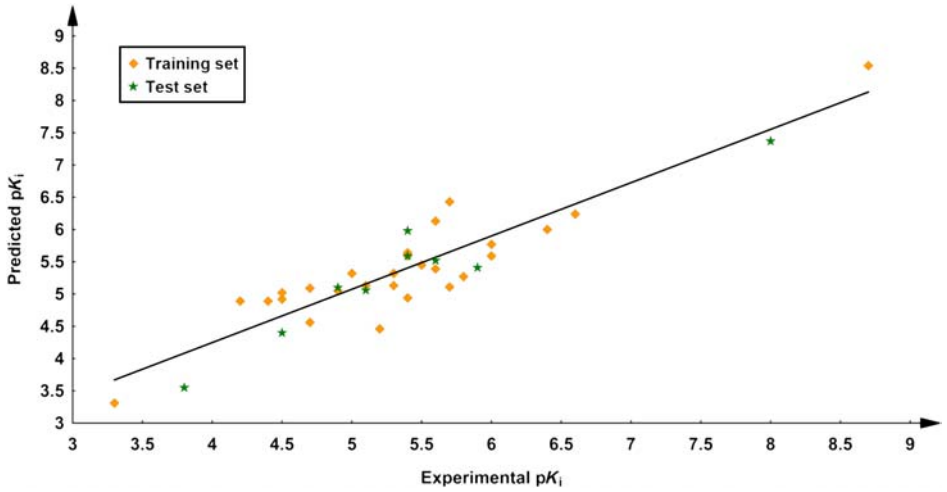

Figure 1. Correlation graph between experimental and predicted activity values for training (square points) and test set (asterisks) compounds based on classical QSAR model.

3.2 3D QSAR model generation

CoMFA and CoMSIA methods were employed to derive 3D QSAR models based on a data-set of 27 compounds for which the HHR1 inverse agonistic activity profile was determined from the same biological assay and used in classical QSAR model generation as discussed earlier. The alignment of these compounds was generated using our previously built pharmacophore model [19]. A number of 3D QSAR models were generated, and the best among them was selected based on the statistically significant results. Though a 3D QSAR model with a q^2 value of >0.4 is normally preferred, a value of >0.3 is also considered statistically significant.

3.2.1 CoMFA study

Force fields are used in CoMFA to describe the interactions that typically occur between a ligand and the target macromolecule. The forces normally responsible for ligand–protein interactions include the steric, electrostatic, hydrogen bonding and hydrophobic molecular fields. The results of CoMFA study are summarised. The best q^2 value 0.580 was obtained from the indicator field with a conventional r^2 value of 0.998, which is a high correlation value along with the low standard error (SE) of estimate (0.050) using seven principal components. The parabolic field has shown the next highest q^2 value (0.573) followed by Tripos standard and hydrogen bonding fields (0.551 and 0.325). The Tripos standard field has produced the highest r^2 value of 1 along with the lowest SE of estimate (0.009) (Table 4). As an indication of statistical significance of the CoMFA model, the biological activity values of the training set compounds were predicted with high correlation (Table 5 and Figure 3). The residual values that were not higher than 0.15 were calculated, and the very high prediction of the training set compounds was proved (Figure 2(b)).

3.2.2 CoMSIA study

Various CoMSIA models were generated considering all possible combinations of field descriptors. Seven CoMSIA fields namely steric (S), electrostatic (E), hydrophobic (H), donor (D), acceptor (A) and combination of SE and AD were used. Among the calculated q^2 values, only steric field has shown a q^2 value of 0.434, which is greater than the preferred value (0.4). None of the other six fields has shown significant values explaining the activity values. The conventional r^2 value for the steric field was 0.862, which was the highest among other fields (Figure 3). Thus, we have considered the CoMSIA steric field model as significant model among others to relate with the biological activities. The experimental activity values of the training set compounds were predicted with high correlation (Table 6) and the residuals were not >0.8, which displays the predictive ability of the model (Figure 2(C)). Further validation analyses based on the test set compounds were carried out for all the models.

3.3 External validation using test set

In order to validate the generated models, an external test set containing nine compounds with considerable diversity in terms of their structures and activity values was used. The activity values of these test set compounds were predicted with high accuracy. The predicted activity values of nine test set compounds based on three models are displayed along with their experimental values in

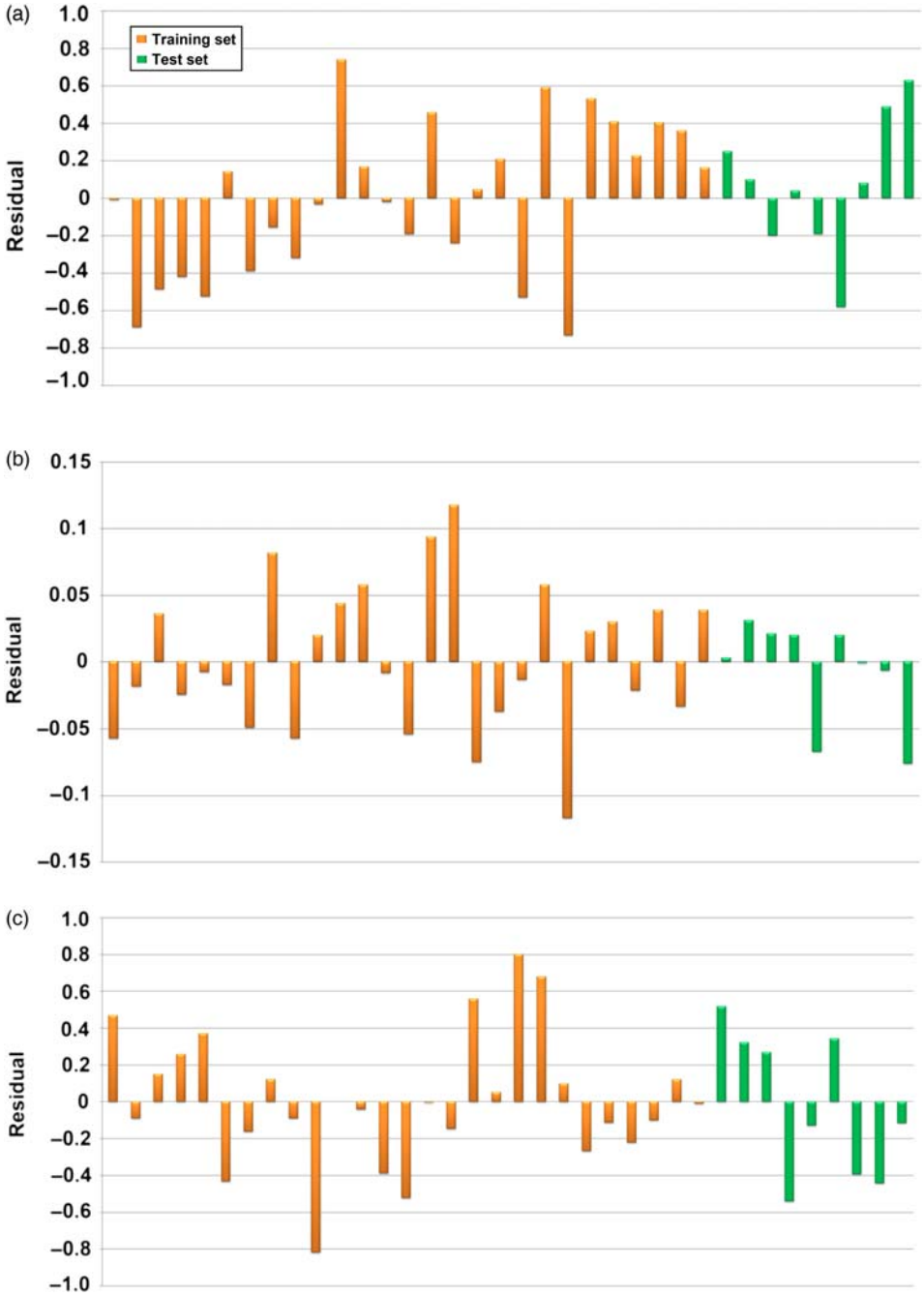

Figure 2. (Colour online). Plot representing the residual values between experimental and predicted activities of training (orange) and test set (green) compounds for (a) classical QSAR, (b) CoMFA and (c) CoMSIA models.

Tables 7 and 8, and a correlation plot was generated between them (Figures 1, 3 and 4). The residual values calculated for all test set compounds from the experimental and predictive activities are plotted as a graph and displayed in Figure 2. The predicted correlation coefficient (r^2_{pred}) value for the classical QSAR model equation is 0.901. The same test set compounds were also used in the validation of CoMFA and CoMSIA models. The r^2_{pred} based on the molecules of test set was calculated by the following equation: $r^2_{\text{pred}} = (\text{SD-PRESS})/\text{SD}$, where SD is the sum of the squared deviations between the biological activities of compounds in the test set and the mean biological activities of the training set compounds and PRESS is the sum of the squared deviations between predicted and actual activity values for each molecule in the test set [50]. The r^2_{pred} value for the test set based on

Table 5. Training set compounds with their experimental, predicted activity values and their residuals predicted from CoMFA and CoMSIA studies.

		CoMFA		CoMSIA	
Comp.	P*K*i (Exp.)	pK_i (Pred.)	Residual	pK_i (Pred.)	Residual
1a	3.3	3.263	−0.037	3.351	0.051
19c	4.2	4.318	0.118	4.053	−0.147
1b	4.4	4.387	−0.013	5.20	0.800
13a	4.5	4.443	−0.057	4.968	0.468
19d	4.5	4.425	−0.075	5.060	0.560
17c	4.7	4.782	0.082	4.820	0.120
1c	4.7	4.758	0.058	5.380	0.680
19b	4.9	4.994	0.094	4.896	−0.004
18f	5	5.044	0.044	5.000	0
13d	5.1	5.136	0.036	5.250	0.150
17a	5.2	5.183	−0.017	4.768	−0.432
13f	5.3	5.276	−0.024	5.558	0.258
1d	5.3	5.183	−0.117	5.399	0.099
13 g	5.4	5.393	−0.007	5.770	0.370
17b	5.4	5.351	−0.049	5.237	−0.163
1i	5.4	5.439	0.039	5.300	−0.100
18 h	5.5	5.492	−0.008	5.110	−0.390
18 g	5.6	5.658	0.058	5.560	−0.040
18i	5.6	5.546	−0.054	5.077	−0.523
18c	5.7	5.643	−0.057	5.610	−0.090
1k	5.7	5.667	−0.033	5.820	0.120
18d	5.8	5.82	0.02	4.980	−0.820
13c	6	5.982	−0.018	5.911	−0.089
1f	6	6.023	0.023	5.732	−0.268
1 g	6.4	6.43	0.03	6.286	−0.114
1 h	6.6	6.579	−0.021	6.378	−0.222
MEP	8.7	8.739	0.039	8.690	−0.010

Notes: MEP – mepyramine. Residual = predicted activity – experimental activity.

CoMFA and CoMSIA studies was 0.998 and 0.897, respectively, which are very high correlation coefficient values.

3.4 CoMFA contour maps

One of the attractive features of the CoMFA and CoMSIA models is the visualisation of the results as 3D coefficient maps. Contour maps were generated from the 3D QSAR models to visualise the information derived and also to rationalise the regions in 3D space around the molecules where changes in each field were predicted to increase or decrease the activity. The 3D QSAR contour maps from both CoMFA and CoMSIA studies clearly illustrate the steric, electrostatic and hydrogen bonding requirements for ligand binding, and provide a deeper visual insight to the medicinal chemists about the SAR. In the CoMFA analysis, sterically unfavourable regions are shown in yellow, whereas favourable regions are in green. Electrostatic positive favourable (or negatively unfavourable) regions correspond to the blue areas, and the negative favourable correspond to the red areas. Analysis of the CoMFA steric and electrostatic fields obtained from the CoMFA indicator field for the most active and least active compounds is shown in Figures 5 and 6. In Figure 5, the green contours represent regions of high steric tolerance (80% contribution), whereas yellow contours represent regions of low steric bulk tolerance (20% contribution). In the same figure, the electrostatic field is indicated by blue (80% contribution) and red (20% contribution) contours that reveal the regions where electron-donating and electron-withdrawing groups would be favourable. As shown in Figure 5(a), the green contour region adjacent to the aromatic ring of MEP indicates that steric bulk is favourable at this region, i.e. substitution on this ring with any bulky groups would

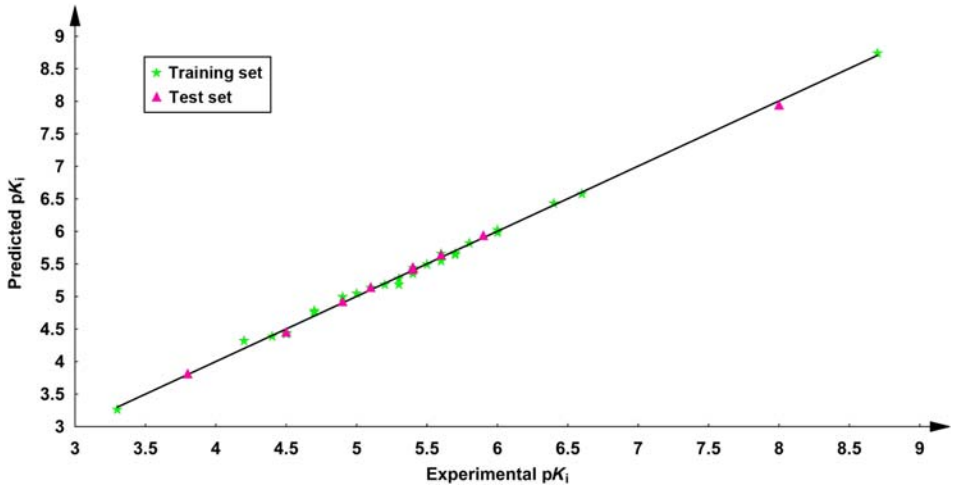

Figure 3. Correlation graph between experimental and predicted activity values for training (asterisks) and test set (triangular points) compounds based on CoMFA model.

Table 6. Summary of PLS statistics of various CoMSIA models using different fields.

Parameters	CM_S	CM_E	CM_A	CM_D	CM_H	CM_SE	CM_AD
q^2	0.434	−0.114	0.120	0.234	0.251	0.194	0.204
r^2	0.862	0.531	0.610	0.560	0.812	0.779	0.625
SE of estimate	0.390	0.719	0.655	0.696	0.454	0.494	0.643
F	66.433	12.068	16.718	13.556	46.187	37.528	17.756
Component	3	1	1	1	1	3	1
Fraction	1	1	1	1	1	0.541(s)	0.663(d)
						0.459(e)	0.337(a)

Notes: CM_S, CM_E, CM_A, CM_D, CM_H, CM_SE, CM_AD – CoMSIA Steric, Electrostatic, Acceptor, Donor, Hydrophobic, Steric & Electrostatic, Acceptor & Donor fields, respectively. s, e, a and d are steric, electrostatic, hydrogen bond acceptor and donor field contributions, respectively.

Table 7. Physicochemical parameters and predicted biological activities for test set compounds based on classical QSAR model (sorted by pK_i values).

Comp.	pK_i (Exp.)	Rings	Q_VSA_PPOS	E_OOP	KierA3	pK_i (Pred.)	Residual
PEA	3.8	1.000	30.430	0.000	1.592	3.55	0.25
19a	4.5	2.000	39.106	0.000	2.197	4.40	0.10
13b	4.9	1.000	30.430	0.000	7.305	5.10	−0.20
18b	5.1	3.000	39.049	0.000	3.276	5.06	0.04
13e	5.4	1.000	30.430	0.000	8.977	5.59	−0.19
1j	5.4	2.000	48.196	0.002	6.656	5.98	−0.58
1e	5.6	1.000	39.049	0.000	7.449	5.52	0.08
18e	5.9	3.000	39.049	0.000	4.561	5.41	0.49
TRN	8	2.000	97.245	0.000	4.044	7.37	0.63

Notes: TRN, Tripelennamine. Residual = predicted activity – experimental activity.

increase the potency of the compound. The huge yellow contour regions along the alkyl-amino chain indicate that bulkier groups would not favour the biological activity. In Figure 5(b), the red contour near the phenyl ring with methoxy group indicates that the electron-withdrawing group would benefit the activity, whereas the blue contour around the rest of the compound demonstrates that electron-donating groups may increase the activity. In Figure 6(a),

Table 8. Prediction of activity values of test set compounds based on CoMFA and CoMSIA models.

		CoMFA		CoMSIA	
Comp.	p*K*i (Expt.)	pK_i (Pred.)	Residual	pK_i (Pred.)	Residual
PEA	3.8	3.794	−0.006	3.356	−0.444
19a	4.5	4.433	−0.067	4.371	−0.129
13b	4.9	4.903	0.003	5.417	0.517
18b	5.1	5.121	0.021	5.368	0.268
13e	5.4	5.431	0.031	5.721	0.321
1j	5.4	5.399	−0.001	5.006	−0.394
1e	5.6	5.62	0.02	5.942	0.342
18e	5.9	5.92	0.02	5.36	−0.54
TRN	8	7.924	−0.076	7.885	−0.115

Notes: TRN, Tripelennamine. Residual = predicted activity – experimental activity. Experimental and predicted activity values are shown along with the residuals.

the steric and electrostatic contour maps for the least active compound in the training set are shown. In order to increase the potency of the least active compound based on the contour maps, steric bulkiness should be increased near the green contour regions, whereas it should be reduced in the yellow regions. In the same way, from Figure 6(b), it was interpreted that the addition of electron-withdrawing groups in the red contour region and addition of electron-donating groups around the blue regions would improve the activity. This is the reason why the compounds MEP and tripelennamine (TRN) are most potent in terms of their antihistaminic activities, since they have the steric bulkiness and electrostatic properties at appropriate regions. The least active compounds with poor activity values possess less or no steric bulkiness and electrostatic properties in the required regions or vice versa. The best CoMSIA models also revealed the same steric and electrostatic regions for most and least active compounds (Figure 7). In Figure 7(a), the steric and electrostatic contours of most active compound MEP are shown, whereas in Figure 7(b), the steric and electrostatic contour maps for the least active compound **1a** are displayed.

4. Conclusion

In this study, during the development of classical QSAR model, four parameters such as Q_VSA_PPOS, E_OOP,

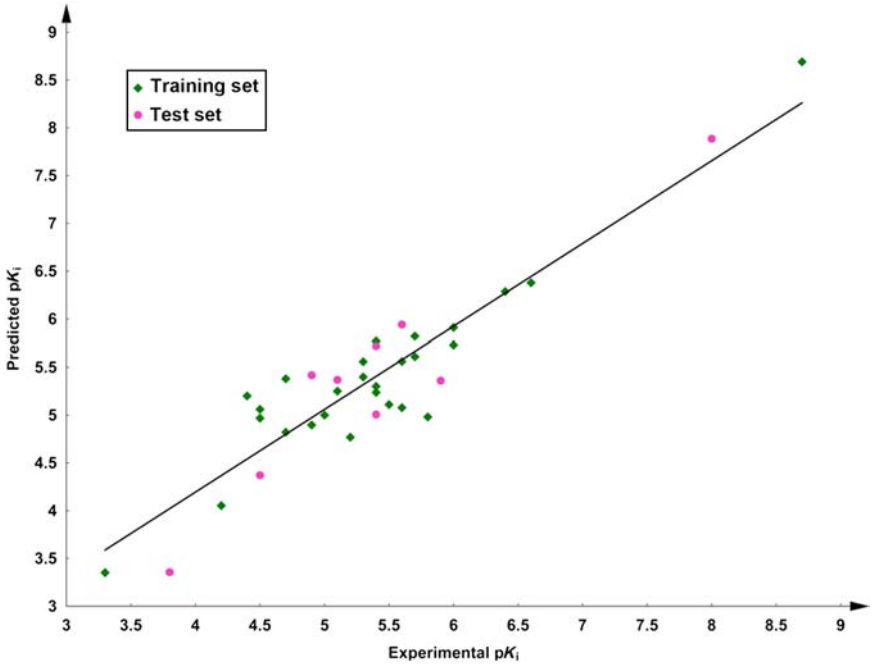

Figure 4. Correlation graph between experimental and predicted activity values for training (squared points) and test set (circular points) compounds based on CoMSIA model.

KierA3 and RINGS explaining polar positive surface area, out-of-plane potential energy, third alpha modified shape index and number of rings, respectively, were involved in the equation and contributed for the HHR1 inverse agonistic activity. The high r^2, q^2 values along with other statistically significant values are the proofs of high predictive ability of the model. The 3D QSAR studies including CoMFA and CoMSIA were carried out using the molecular alignment derived based on our pharmacophore model containing five features. The CoMFA indicator and parabolic fields predicted the activity values with q^2values of 0.580 and 0.573, respectively. Analyses of contour maps generated using CoMFA and CoMSIA models revealed the contribution of steric and electrostatic fields around the molecules that would in turn help medicinal chemists to design new compounds by understanding the effects of steric and electrostatic properties on binding affinity.

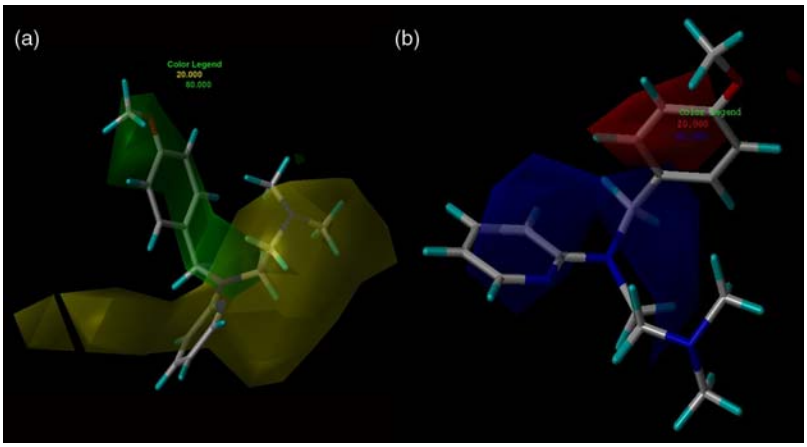

Figure 5. (Colour online) Graphical representation of best CoMFA models at the default resolution of 80% favoured and 20% disfavoured regions. (a) steric fields and (b) electrostatic fields around the most active compound MEP.

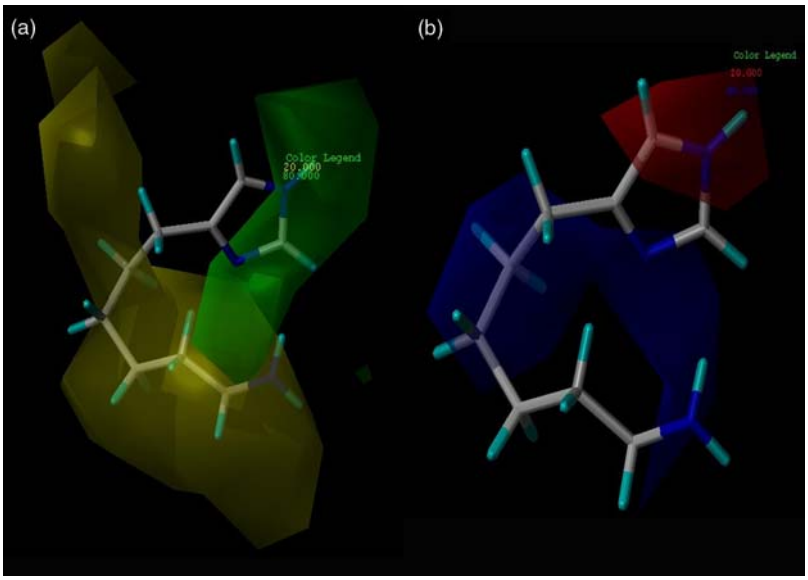

Figure 6. (Colour online) Graphical representation of best CoMFA models at the default resolution of 80% favoured and 20% disfavoured regions. (a) steric fields and (b) electrostatic fields around the least active compound **1a**.

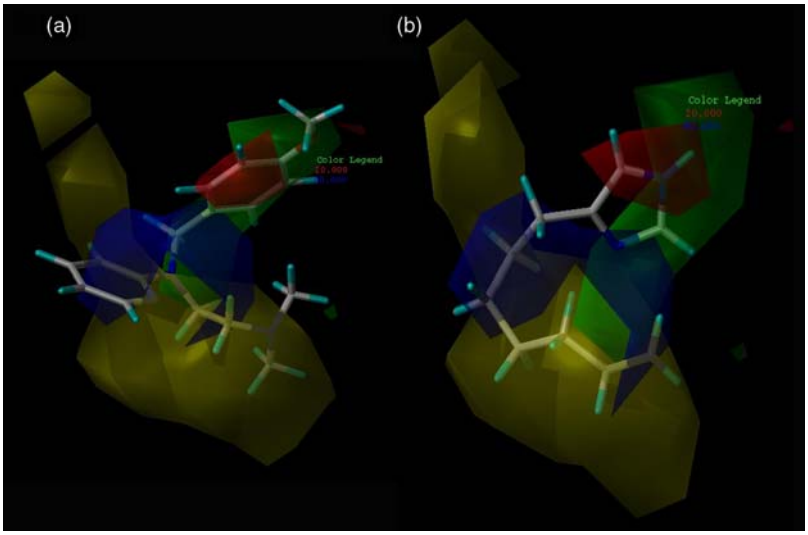

Figure 7. (Colour online) Graphical representation of best CoMSIA models at the default resolution of 80% favoured and 20% disfavoured regions. (a) steric and electrostatic fields around MEP and (b) steric and electrostatic fields around the least active compound **1a**.

Acknowledgements

This research was supported by Basic Science Research Program (2009-0073267), Pioneer Research Center Program (2009-0081539) and Management of Climate Change Program (2010-0029084) through the National Research Foundation of Korea (NRF) funded by the Ministry of Education, Science and Technology (MEST) of Republic of Korea. This work was also supported by the Next-Generation BioGreen 21 Program (PJ008038) from Rural Development Administration (RDA) of Republic of Korea. The authors would like to thank Central Drug Research Institute, Lucknow, India, for financial support. Dr A.K. Saxena, Dr Anshuman Dixit and A.S. Kushwaha are gratefully thanked for their assistance during this work.

References

[1] V. Jitender, M.K. Vijay, and C.C. Evans, *3D-QSAR in drug design – a review*, Curr. Top. Med. Chem. 10 (2010), pp. 95–115.
[2] M. Akamatsu, *Current state and perspectives of 3D-QSAR*, Curr. Top. Med. Chem. 2 (2002), pp. 1381–1394.
[3] A.J. Hopfinger and J.S. Tokarski, *Three-dimensional quantitative structure–activity relationship analysis*, in *Practical Application of Computer-Aided Drug Design*, P.S. Charifson, ed., Marcel Dekker, Inc., New York, 1997, pp. 105–164.
[4] Y.C. Martin, *3D QSAR: Current state, scope, and limitations*, in *3D QSAR in Drug Design – Recent Advances*, H. Kubinyi, G. Folkers, and Y.C. Martin, eds., Kluwer Academic Publishers, New York, 1998, pp. 3–23.

[5] P. Matyus and A.P. Borosy, *Three dimensional structure–activity relationships*, Acta Pharm. Hung. 68 (1998), pp. 33–38.

[6] S.J. Hill, C.R. Ganellin, H. Timmerman, J.C. Schwartz, N.P. Shankley, J.M. Young, W. Schunack, R. Levi, and H.L. Haas, *International union of pharmacology XIII, classification of histamine receptors*, Pharmacol. Rev. 49 (1997), pp. 253–278.

[7] M.D. De Backer, W. Gommeren, H. Moereels, G. Nobels, P. van Gompel, J.E. Leysen, and W.H. Luyten, *Genomic cloning, heterologous expression and pharmacological characterization of a human histamine H_1 receptor*, Biochem. Biophys. Res. Commun. 197 (1993), pp. 1601–1608.

[8] H. Fukui, K. Fujimoto, H. Mizuguchi, K. Sakamoto, Y. Horio, S. Takai, K. Yamada, and S. Ito, *Molecular cloning of the human histamine H_1 receptor gene*, Biochem. Biophys. Res. Commun. 201 (1994), pp. 894–901.

[9] N. Moguilevsky, F. Varsalona, M. Noyer, M. Gillard, J.P. Guillaume, L. Garcia, C. Szpirer, J. Szpirer, and A. Bollen, *Stable expression of human H_1-histamine-receptor cDNA in Chinese hamster ovary cells, pharmacological characterisation of the protein, tissue distribution of messenger RNA and chromosomal localisation of the gene*, Eur. J. Biochem. 224 (1994), pp. 489–495.

[10] I. Gantz, G. Munzert, T. Tashiro, M. Schaffer, L. Wang, V.J. Del, and T. Yamada, *Molecular cloning of the human histamine H_2 receptor*, Biochem. Biophys. Res. Commun. 178 (1991), pp. 1386–1392.

[11] T.W. Lovenberg, B.L. Roland, S.J. Wilson, X. Jiang, J. Pyati, A. Huvar, M.R. Jackson, and M.G. Erlander, *Cloning and functional expression of the human histamine H_3 receptor*, Mol. Pharmacol. 55 (1999), pp. 1101–1107.

[12] Y. Zhu, D. Michalovich, H.L. Wu, K.B. Tan, G.M. Dytko, I.J. Mannan, R. Boyce, J. Alston, L.A. Tierney, X. Li, N.C. Herrity, L. Vawter, H.M. Sarau, R.S. Ames, C.M. Davenport, J.P. Hieble, S. Wilson, D.J. Bergsma, and L.R. Fitzgerald, *Cloning, expression, and pharmacological characterization of a novel human histamine receptor*, Mol. Pharmacol. 59 (2001), pp. 434–441.

[13] C. Liu, X.J. Ma, X. Jiang, S.J. Wilson, C.L. Hofstra, J. Blevitt, J. Pyati, X. Li, W. Chai, N. Carruthers, and T.W. Lovenberg, *Cloning and pharmacological characterization of a fourth histamine receptor H_4 expressed in bone marrow*, Mol. Pharmacol. 59 (2001), pp. 420–426.

[14] T. Oda, N. Morikawa, Y. Saito, Y. Masuho, and S. Matsumoto, *Molecular cloning and characterization of a novel type of histamine receptor preferentially expressed in leukocytes*, J. Biol. Chem. 275 (2000), pp. 36781–36786.

[15] T. Nakamura, H. Itadani, Y. Hidaka, M. Ohta, and K. Tanaka, *Molecular cloning and characterization of a new human histamine H_4 receptor*, Biochem. Biophys. Res. Commun. 279 (2000), pp. 615–620.

[16] K.L. Morse, J. Behan, T.M. Laz, R.E. West, S.A. Greenfeder, J.C. Anthes, S. Umland, Y. Wan, R.W. Hipkin, W. Gonsiorek, N. Shin, E.L. Gustafson, X. Qiao, S. Wang, J.A. Hedrick, J. Greene, M. Bayne, and F.J. Monsma, *Cloning and characterization of a novel human histamine receptor*, J. Pharmacol. Exp. Ther. 296 (2001), pp. 1058–1066.

[17] H.H. Dale and P.P. Laidlaw, *The physiological action of β-imidazolylethylamine*, J. Physiol. 41 (1910), pp. 318–344.

[18] M.Q. Zhang, R. Leurs, and H. Timmerman, *Histamine H_1-receptor antagonists*, *Burger's Medicinal Chemistry and Drug Discovery*, 5th ed., John Wiley & Sons, New York, 1997, pp. 495–559.

[19] S. Thangapandian, N. Krishnamoorthy, S. John, S. Sakkiah, P. Lazar, Y. Lee, and K.W. Lee, *Pharmacophore modeling, virtual screening and molecular docking studies for identification of new inverse agonists of human histamine H1 receptor*, Bull. Korean Chem. Soc. 31 (2010), pp. 1–7.

[20] M. Kakiuchi, T. Ohashi, K. Musoh, K. Kawamura, K. Morikawa, and H. Kato, *Studies on the novel antiallergic agent hsr-609: Its penetration into the central nervous system in mice and guinea pigs and its selectivity for the histamine H1-receptor*, Jpn. J. Pharmacol. 73 (1997), pp. 291–298.

[21] B.C. Sangalli, *Role of the central histaminergic neuronal system in the CNS toxicity of the first generation H1-antagonists*, Prog. Neurobiol. 52 (1997), pp. 145–157.

[22] M.J. Welch, E.O. Meltzer, and F.E.R. Simons, *H1-antihistamines and the central nervous system. Histamine and H1-Antihistamines in Allergic Disease*, F.E.R. Simons, ed., Marcel Dekker, New York, 2002, pp. 337–388.

[23] F.E.R. Simons and K.J. Simons, *Clinical pharmacology of new histamine H1 receptor antagonists*, Clin. Pharmacokinet. 36 (1999), pp. 329–352.

[24] H. Timmerman, G.M. Walsh, L. Annunziato, N. Frossard, K. Knol, S. Levander, J.M. Nicolas, M. Taglialatela, M.D. Tharp, and J.P. Tillement, *New insights into the second generation anti-histamines*, Drugs 61 (2001), pp. 207–236.

[25] H. Nonaka, S. Otaki, E. Ohshima, M. Kono, H. Kase, K. Ohta, H. Fukui, and M. Ichimura, *Unique binding pocket for KW-4679 in the histamine H1 receptor*, Eur. J. Pharmacol. 345 (1998), pp. 111–117.

[26] T. Costa, Y. Ogino, P.J. Munson, H.O. Onaran, and D. Rodbard, *Drug efficacy at guanine nucleotide-binding regulatory protein-linked receptors: Thermodynamic interpretation of negative antagonism and of receptor activity in the absence of ligand*, Mol. Pharmacol. 41 (1992), pp. 549–560.

[27] W. Schutz and M. Freissmuth, *Reverse intrinsic activity of antagonists on G protein-coupled receptors*, Trends Pharmacol. Sci. 13 (1992), pp. 376–380.

[28] R.J. Lefkowitz, S. Cotecchia, P. Samama, and T. Costa, *Constitutive activity of receptors coupled to guanine nucleotide regulatory proteins*, Trends Pharmacol. Sci. 14 (1993), pp. 303–307.

[29] G. Milligan, R.A. Bond, and M. Lee, *Inverse agonism: Pharmacological curiosity or potential therapeutic strategy?* Trends Pharmacol. Sci. 16 (1995), pp. 10–13.

[30] T. Kenakin, *The classification of seven transmembrane receptors in recombinant expression systems*, Pharmacol. Rev. 48 (1996), pp. 413–463.

[31] A. Shenker, L. Laue, S. Kosugi, J.J. Merendino, Jr, T. Minegishi, and G.B. Cutler, Jr, *A constitutively activating mutation of the luteinizing hormone receptor in familial male precocious puberty*, Nature (London) 365 (1993), pp. 652–654.

[32] P.R. Robinson, G.B. Cohen, E.A. Zhukovsky, and D.D. Oprian, *Constitutively active mutants of rhodopsin*, Neuron 9 (1992), pp. 719–725.

[33] J. Parma, L. Duprez, J. Van Sande, P. Cochaux, C. Gervy, J. Mockel, J. Dumont, and G. Vassart, *Somatic mutations in the thyrotropin receptor gene cause hyperfunctioning thyroid adenomas*, Nature (London) 365 (1993), pp. 649–651.

[34] L.S. Robbins, J.H. Nadeau, K.R. Johnson, M.A. Kelly, L. Roselli-Rehfuss, E. Baack, K.G. Mountjoy, and R.D. Cone, *Pigmentation phenotypes of variant extension locus alleles result from point mutations that alter MSH receptor function*, Cell 72 (1993), pp. 827–834.

[35] M. Govoni, R.A. Bakker, I. van de Wetering, M.J. Smit, W.M. Menge, H. Timmerman, S. Elz, W. Schunack, and R. Leurs, *Synthesis and pharmacological identification of neutral histamine H1-receptor antagonists*, J. Med. Chem. 46 (2003), pp. 5812–5824.

[36] L. Paul, *A widely applicable set of descriptors*, J. Mol. Graph. Model. 18 (2000), pp. 464–477.

[37] B. Paul, *A review of the SYSTAT v.10.2 software package*, Br. J. Math. Stat. Psychol. 56 (2003), pp. 189–195.

[38] B.O. Daniel and C.G. Anderson, *BuildQSAR: A new program for QSAR analysis*, Quant. Struct. Act. Relat. 19 (2000), pp. 599–601.

[39] R.A. Berk, *The formalities of multiple regression*, in *Regression Analysis: A Constructive Critique*, R.A. Berk, ed., SAGE Publications Ltd, London, 2003, pp. 103–110.

[40] R.A. Berk, *Some popular extensions of multiple regression*, in *Regression Analysis: A Constructive Critique*, R.A. Berk, ed., SAGE Publications Ltd, London, 2003, pp. 125–150.

[41] A.K. Gupta and A.K. Saxena, *3D-QSAR CoMFA and CoMSIA studies on a set of diverse α_{1a}-adrenergic receptor antagonists*, Med. Chem. Res, doi: 10.1007/s00044-010-9379-1.

[42] A. Dixit, S.K. Kashaw, S. Gaur, and A.K. Saxena, *Development of CoMFA, advance CoMFA and CoMSIA models in pyrroloquinazolines as thrombin receptor antagonist*, Bioorg. Med. Chem. 12 (2004), pp. 3591–3598.

[43] F.A. Pasha, M. Muddassar, H. Jung, Y. Beom-Seok, L. Cheolju, S.O. Jung, J.C. Seung, and C. Hoon, *QM and pharmacophore based*

3D-QSAR of MK886 analogues against mPGES-1, Bull. Korean Chem. Soc. 29 (2008), pp. 647–655.

[44] K. Shantaram and K.B. John, *Receptor-guided alignment-based comparative 3D-QSAR studies of benzylidene malonitrile tyrphostins as EGFR and HER-2 kinase inhibitors*, J. Med. Chem. 46 (2003), pp. 4657–4668.

[45] D.M. Varnavas, M.M. Thomas, and K. George, *Molecular docking and 3D-QSAR CoMFA studies on indole inhibitors of GIIA secreted phospholipase A2*, J. Chem. Inf. Model. 50 (2010), pp. 1589–1601.

[46] K. Jinyoung, H.H. Jin, and C. Youhoon, *A structure-based 3D-QSAR (CoMSIA) study on a series of aryl diketoacids (ADK) as inhibitors of HCV RNA-dependent RNA polymerase*, Bull. Korean Chem. Soc. 27 (2006), pp. 1919–1922.

[47] K.H. Kim, *Comparative molecular field analysis (CoMFA)*, in *Molecular Similarity in Drug Design*, P.M. Dean, ed., Blackie Academic & Professional, Glasgow, 1995, pp. 291–331.

[48] T.I. Oprea, *3D QSAR modeling in drug design*, in *Computational Medicinal Chemistry for Drug Discovery*, P. Bultinck, H.D. Winter, W. Langenaeker, and J.P. Tollenaere, eds., Marcel Dekker, Inc., New York, 2004, pp. 571–616.

[49] S. Wold, E. Johansson, and M. Cocchi, *PLS: Partial least squares projections to latent structures*, in *3D QSAR in Drug Design: Theory, Methods and Applications*, H. Kubinyi, ed., ESCOM Science Publishers, Leiden, 1993, pp. 523–550.

[50] L. Ping, H. Zhi-Jian, S. Jun-Rong, and C. Wei-Min, *3D-QSAR and molecular docking studies on fused pyrazoles as p38α mitogen-activated protein kinase inhibitors*, Int. J. Mol. Sci. 11 (2010), pp. 3357–3374.